



Analysis of low efficiency droop of semipolar InGaN quantum well light-emitting diodes by modified rate equation with weak phase-space filling effect

Houqiang Fu, Zhijian Lu, and Yuji Zhao

Citation: *AIP Advances* **6**, 065013 (2016); doi: 10.1063/1.4954296

View online: <http://dx.doi.org/10.1063/1.4954296>

View Table of Contents: <http://scitation.aip.org/content/aip/journal/adva/6/6?ver=pdfcov>

Published by the *AIP Publishing*

Articles you may be interested in

[Spatially resolved study of quantum efficiency droop in InGaN light-emitting diodes](#)

Appl. Phys. Lett. **101**, 252103 (2012); 10.1063/1.4772549

[Analysis of efficiency droop in nitride light-emitting diodes by the reduced effective volume of InGaN active material](#)

Appl. Phys. Lett. **100**, 131109 (2012); 10.1063/1.3698113

[Rate equation analysis of efficiency droop in InGaN light-emitting diodes](#)

Appl. Phys. Lett. **95**, 081114 (2009); 10.1063/1.3216578

[Effect of electron blocking layer on efficiency droop in InGaN/GaN multiple quantum well light-emitting diodes](#)

Appl. Phys. Lett. **94**, 231123 (2009); 10.1063/1.3153508

[Reduction of efficiency droop in InGaN light emitting diodes by coupled quantum wells](#)

Appl. Phys. Lett. **93**, 171113 (2008); 10.1063/1.3012388

The advertisement features a blue background with a glowing light effect. On the left is a thumbnail of an 'Applied Physics Reviews' journal cover showing a diagram of a quantum well structure. The main text reads 'NEW Special Topic Sections' in large white letters. Below this, it says 'NOW ONLINE' in yellow, followed by 'Lithium Niobate Properties and Applications: Reviews of Emerging Trends' in white. The AIP Applied Physics Reviews logo is in the bottom right corner.

NEW Special Topic Sections

NOW ONLINE
Lithium Niobate Properties and Applications:
Reviews of Emerging Trends

AIP Applied Physics Reviews

Analysis of low efficiency droop of semipolar InGaN quantum well light-emitting diodes by modified rate equation with weak phase-space filling effect

Houqiang Fu, Zhijian Lu, and Yuji Zhao

School of Electrical, Computer and Energy Engineering, Arizona State University,
Tempe, AZ 85287, U.S.A.

(Received 17 April 2016; accepted 8 June 2016; published online 15 June 2016)

We study the low efficiency droop characteristics of semipolar InGaN light-emitting diodes (LEDs) using modified rate equation incorporating the phase-space filling (PSF) effect where the results on c -plane LEDs are also obtained and compared. Internal quantum efficiency (IQE) of LEDs was simulated using a modified ABC model with different PSF filling (n_0), Shockley-Read-Hall (A), radiative (B), Auger (C) coefficients and different active layer thickness (d), where the PSF effect showed a strong impact on the simulated LED efficiency results. A weaker PSF effect was found for low-droop semipolar LEDs possibly due to small quantum confined Stark effect, short carrier lifetime, and small average carrier density. A very good agreement between experimental data and the theoretical modeling was obtained for low-droop semipolar LEDs with weak PSF effect. These results suggest the low droop performance may be explained by different mechanisms for semipolar LEDs. © 2016 Author(s). All article content, except where otherwise noted, is licensed under a Creative Commons Attribution (CC BY) license (<http://creativecommons.org/licenses/by/4.0/>). [<http://dx.doi.org/10.1063/1.4954296>]

I. INTRODUCTION

Efficiency droop, referring the reduction of efficiency with increasing current density in InGaN based LEDs,^{1,2} has been one of the biggest problem hindering the fast adoption of LED technology in solid state lighting and displays. Mechanisms such as Auger recombination,^{3,4} quantum confined Stark effect,⁵ and carrier leakage³ have been studied to explain the efficiency droop. Successful analysis of the physical mechanisms can also contribute to improving other InGaN based optoelectronics, such as photovoltaics.⁶ However the actual reason is not conclusive yet. The droop characteristic of LEDs is generally characterized by carrier rate equation model with ABC coefficients, where A , B , and C are Shockley-Read-Hall (SRH), radiative, and Auger coefficients, respectively. Recently, direct experimental evidence of Auger scattering from an InGaN LED under electrical injection was reported using electron emission spectroscopy, which is in strong support for the Auger hypotheses.⁷ However, one of the major drawbacks for the Auger recombination theory is that the theoretical C coefficient obtained by the direct intraband Auger recombination process is too low to account for the observed experimental results.^{8,9} In order to overcome this discrepancy in ABC model, many efforts have been developed from different perspectives. For example, Kioupakis *et al* studied indirect Auger recombination process mediated by electron-phonon coupling and alloy scattering using atomistic first-principle calculations and obtained a larger C coefficient.¹⁰ Ryu *et al* showed that the combination of indium composition fluctuation, internal polarization and inhomogeneous carrier distribution lead to reduced active region volume which will affect the ABC model and therefore impact the droop properties.¹¹ In an analytic model, Lin *et al* modified the ABC equation where a drift-induced leakage (C_{DL}) term was incorporated into the C coefficient along with the Auger (C_{Auger}) term.¹² However, most of these analyses are almost exclusively based on the conventional c -plane devices.

Recently, nonpolar and semipolar InGaN LEDs have been proposed to solve the efficiency droop problem.^{13–19} It is argued that reduced or eliminated polarization-related effects in semipolar



or nonpolar GaN enables the growth of thick heterostructures or quantum wells (QWs), which results in reduced carrier density in the active layer and thus less droop effect. It's have been reported that semipolar $(20\bar{2}1)$ and $(30\bar{3}1)$ LEDs have superior low droop performance.¹³⁻¹⁵ Furthermore, a recent study compared internal quantum efficiencies (IQEs) of semipolar and conventional c -plane InGaN LEDs using a modified ABC model with PSF effect developed by David *et al.*^{20,21} Later on Kioupakis et al found that PSF can severely lower the LEDs efficiency using first-principle calculation.²² Although the IQE curve of c -plane devices was very well fitted with the model, similar A, B, C coefficients were not able to model the semipolar LEDs.²¹ These results indicate that a different ABC model has to be used for nonpolar and semipolar LEDs where the different physical properties and resulted carrier dynamics must be taken in to account. In this paper, we study the phase-space filling (PSF) effect on the modelling of semipolar InGaN LEDs. A much weaker phase-space filling was found on semipolar LEDs possibly due to the lower carrier density in the devices. The modified ABC equation shows good agreement with experimental results on semipolar LEDs.

II. SIMULATION METHODS

A. Modified rate equations

For c -plane devices, it was argued that the decreasing of B and C coefficient at high carrier density in c -plane LED is accounted by strong PSF effect due to the invalidity of Boltzmann distribution caused by Pauli exclusion principle.²³ Based on these considerations, the current density J and IQE can be written as a function of carrier density n ²⁰:

$$J = qd (An + Bn^2/(1 + n/n_0) + Cn^3/(1 + n/n_0)) \quad (1)$$

$$IQE = Bn^2/(1 + n/n_0) / [An + Bn^2/(1 + n/n_0) + Cn^3/(1 + n/n_0)] \quad (2)$$

where q is the charge of electron and d is the active region thickness. n_0 is the phase-space filling coefficient, and $B/(1 + n/n_0)$ and $C/(1 + n/n_0)$ are radiative and Auger coefficients with PSF effect. From the equations, it indicates that smaller n_0 means strong PSF effect. For nonpolar and semipolar devices, however, carrier density can be much lower due to several mechanisms, which will potentially impact the PSF effect. These physical mechanisms will be examined in the second part of the paper. To study the PSF effect on the LEDs droop performance, we calculate the IQE curves for LED structure with different A, B, C, d and n_0 coefficients based on Eqs. (1) and (2) (which are also called rate equation model).

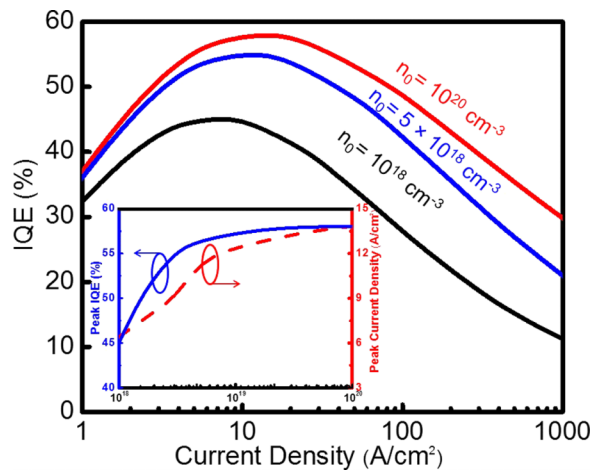


FIG. 1. Calculated IQE curves as a function of current density with different n_0 coefficients. The inset presents the calculated peak IQEs and peak current densities of LEDs as a function of n_0 coefficient.

TABLE I. Droop ratio (%) for IQE curve with different n_0 at different current densities.

n_0/cm^3	100 A/cm ²	200 A/cm ²	300 A/cm ²	400 A/cm ²
10^{18}	38.4	51.1	58.2	62.4
5×10^{18}	23.1	35.1	43.6	47.0
10^{20}	15.5	25.0	31.5	35.3

B. Droop performance

IQE curves as a function of current densities are calculated in Figure 1. The A , B , C and d values used in the calculations are $1 \times 10^7 \text{ s}^{-1}$, $2 \times 10^{-11} \text{ cm}^3 \cdot \text{s}^{-1}$, $5 \times 10^{-30} \text{ cm}^6 \cdot \text{s}^{-1}$ and 12 nm (4 sets of QWs with 3 nm each), respectively, which are reasonable values for InGaN LEDs. High C coefficient used based on experimental results to account for both direct and indirect Auger process.^{3,6-8} The simulated results show that n_0 has strong impacts on both the peak IQE and the efficiency droop of the LEDs. The absolute IQE values increases when n_0 increases, indicating that a weaker PSF effect will lead to a higher IQE value at all current densities. The inset demonstrates the peak IQE (solid blue line) and peak current density (dash red line) as a function of n_0 . The results show that the peak IQE and peak current density first rise up with increasing n_0 and then saturates at around $n_0 = 10^{20} \text{ cm}^{-3}$. However, when n_0 exceeds 10^{20} cm^{-3} , PSF effect shows almost no impact. This is possibly due to the fact that PSF only comes into play when $n/n_0 \approx 1$, as indicated in Eqs. (1) and (2). When n_0 is larger than 10^{20} cm^{-3} , $n/n_0 \ll 1$ and therefore the PSF effect is minimum. Furthermore, we discuss the PSF effect on the efficiency droop, where the droop ratios for IQE curves with different n_0 are summarized in Table I. The droop ratio is defined as droop ratio = $(\text{IQE}_{\text{Max}} - \text{IQE}_J) / \text{IQE}_{\text{Max}} \times 100\%$, where the IQE_{Max} and IQE_J represent the IQE maximum and the IQE at different current densities. For $n_0 = 10^{18} \text{ cm}^{-3}$, the IQE curve exhibits 38.4% efficiency droop at a current density of 100 A/cm² and a very large droop of 62.4% at a current density of 400 A/cm². When n_0 increases, the droop ratio of the devices decreases due to the decreased PSF effect. For $n_0 = 10^{20} \text{ cm}^{-3}$, the droop is only 15.5% and 35.3% for a current density of 100 A/cm² and 400 A/cm², respectively. This indicates that weaker PSF effect will also lead to lower efficiency droop especially at high current density.

Figures 2(a)-2(c) present IQE curve versus current density with different A , B , and C coefficients. In order to investigate the influence of PSF effect in detail, IQE curves with strong PSF ($n_0 = 3 \times 10^{18} \text{ cm}^{-3}$) are compared with that of weak PSF ($n_0 = 5 \times 10^{19} \text{ cm}^{-3}$) here. In Fig. 4(a), IQE curve is calculated with various A coefficients while B ($2 \times 10^{-11} \text{ cm}^3 \cdot \text{s}^{-1}$) and C ($3 \times 10^{-30} \text{ cm}^6 \cdot \text{s}^{-1}$) and d (18 nm) are kept the same. It shows that strong PSF effect reduces IQE at certain current density and IQE difference between strong and weak PSF effect is particularly prominent at high current density, which can be more than 20%. It is also noteworthy that a strong PSF effect will give rise to smaller peak IQE and peak current density. Similar tendencies were also observed for different B and C coefficients as indicated in Figs. 2(b) and 2(c). The simulated results show that the PSF effect has strong influences in IQE under different radiative recombination (B) process and Auger recombination (C) process. However, A is less affected compared to B and C due

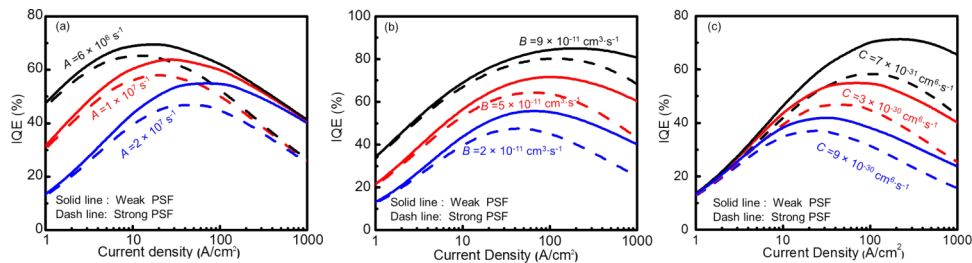


FIG. 2. Calculated IQE curves as a function of current density with weak PSF effect (solid line, $n_0 = 5 \times 10^{19} \text{ cm}^{-3}$) and strong PSF effect (dash line, $n_0 = 3 \times 10^{18} \text{ cm}^{-3}$) varying (a) A coefficient, (b) B coefficient, (c) C coefficient.

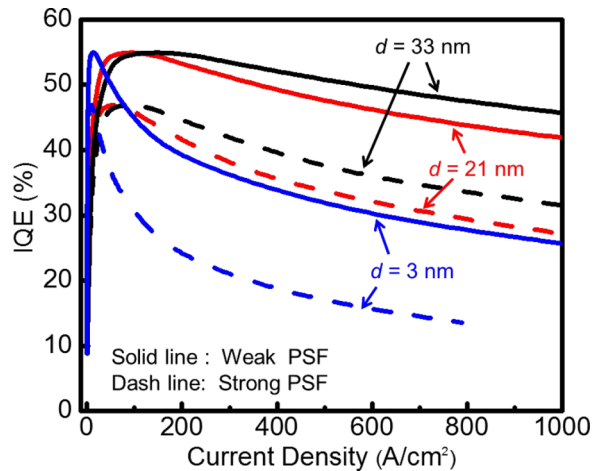


FIG. 3. Calculated IQE curves as a function of current density with weak PSF effect (solid line, $n_0 = 5 \times 10^{19} \text{ cm}^{-3}$) and strong PSF effect (dash line, $n_0 = 3 \times 10^{18} \text{ cm}^{-3}$) with different active layer thickness d .

to the fact that A is mainly concerned at low current density region. This is also consistent with rate equation mentioned above.

Figure 3 demonstrates IQE versus current density with different active region thickness for both strong PSF ($n_0 = 3 \times 10^{18} \text{ cm}^{-3}$) and weak PSF ($n_0 = 5 \times 10^{19} \text{ cm}^{-3}$) effects. The AB and C coefficients are kept as $2 \times 10^7 \text{ s}^{-1}$, $2 \times 10^{-11} \text{ cm}^3 \cdot \text{s}^{-1}$, $3 \times 10^{-30} \text{ cm}^6 \cdot \text{s}^{-1}$, respectively. The thickness of the active region d is set as 3 nm (1 set of QWs), 21 nm (7 sets of QWs) and 33 nm (11 sets of QWs), respectively. The calculation shows that an increasing active region thickness will effectively reduce the efficiency droop, which is consistent with other theoretical studies and experimental results. However, at same active region thickness, the structures with a strong PSF effect will result in a significant reduced IQE (as high as 15%) at certain current density comparing with that of the structures with weak PSF effect.

C. Physical mechanism

LEDs structures with strong (polar c -plane devices) and weak (nonpolar/semipolar devices) PSF effect will have very different IQE curve and droop characteristics. The modeling of such devices should be therefore treated differently. This concept may explain the different efficiency droop characteristics in polar c -plane LEDs and nonpolar/semipolar LEDs, where the experimental data on c -plane (nonpolar/semipolar) structures showed similar IQE characteristics with the simulated results on strong (weak) PSF effect. The physical origin of such difference in PSF effect can be explained in several perspectives.

First of all, for c -plane devices, strong polarization-induced electric field exists inside the In-GaN QWs, which will result in significant energy band tilting which leads to a phenomenon known as quantum-confined Stark effect (QCSE). This distorted band diagram will greatly decrease the electron and hole's wavefunction overlap (as shown in Fig. 4(a)). Kioupakis *et al* shows that the radiative recombination coefficient is proportional to the square of the wavefunction overlap.²⁴ Thus a less wavefunction overlap in c -plane LEDs will lead to a lower radiative recombination rate (B). Further theoretical and experimental work show that A and C are also related to the squared of the wavefunction overlap.^{21,25} These results mean at certain current density, semipolar LEDs has higher A , B and C coefficients than c -plane LEDs. Though higher current density can reduce the QCSE, calculations show that the square of wavefunction overlap of semipolar planes are always higher than that of c -plane at all current densities.²⁶ Therefore the reduction of QCSE at high current density has minimum effect on the droop characteristics of semipolar and c -plane LEDs. Since A , B , and C coefficients are smaller for c -plane LEDs, the carrier density is always higher at a given current density on this polar orientation according to Eq. (1). This results in a strong PSF effect in c -plane LEDs.

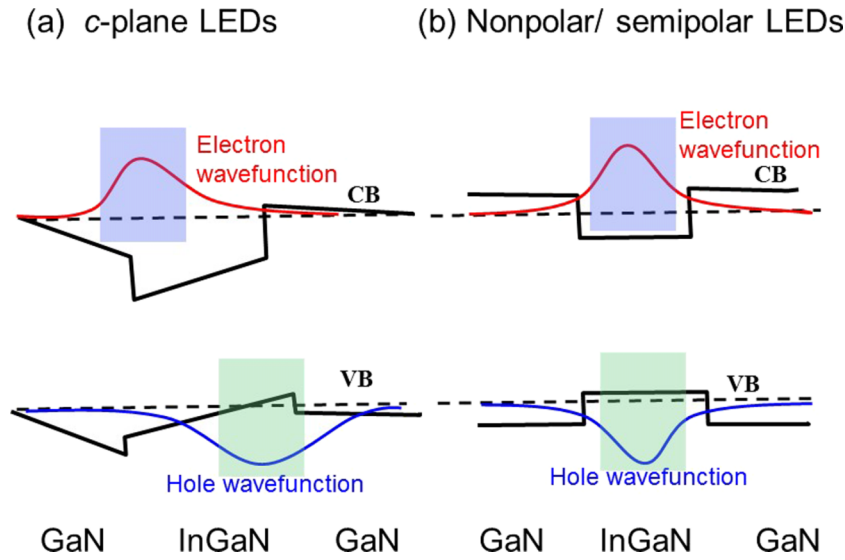


FIG. 4. Schematic band diagram and electron and hole wavefunction of (a) *c*-plane InGaN LEDs and (b) nonpolar/semipolar InGaN LEDs.

In contrast, nonpolar or semipolar InGaN QWs have eliminated or reduced QCSE (Fig. 4(b)), which will lead to a flatter QW profile and higher wavefunction overlap, and a lower carrier density (weak PSF effect).

Secondly, short carrier lifetime and faster carrier transport may also contribute to a weaker PSF effect for semipolar LEDs. Figure 5 shows the time-resolved photoluminescence measurements

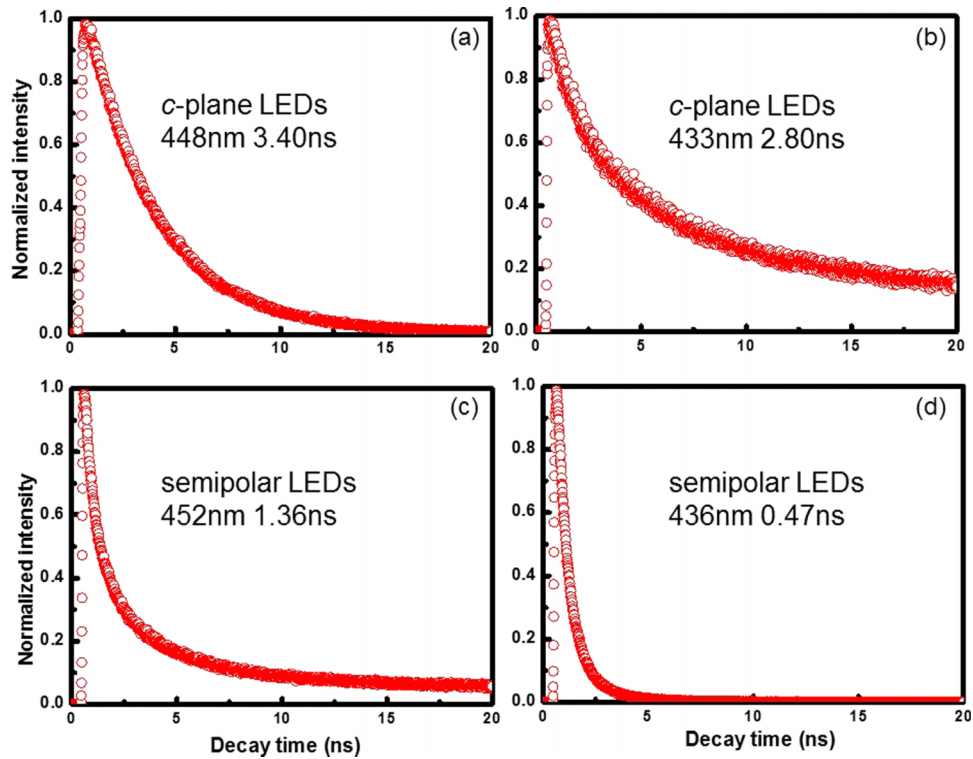


FIG. 5. (a) Signals of time resolved photoluminescence for *c*-plane (a & b) and semipolar LEDs (c & d). Carrier lifetime is obtained by exponential fitting. And the peak wavelength of photoluminescence of these samples are also shown.

(TRPL) for both *c*-plane and semipolar (20 $\bar{2}$ 1) LEDs. These LEDs are grown by conventional metalorganic chemical vapor deposition (MOCVD) with similar device structures, i.e. three 3nm InGaN/12nm GaN QWs with indium composition around 12%. The details about the growth can be found in Refs. 25 and 27. TRPL measurement is carried at 300K using a time-correlated single photon counting (TCSPC) system. The excitation laser wavelength is 390nm. And the power is set to 0.1mW in order to ensure low injection which avoids affecting the internal electric field of the QW so that the intrinsic properties of different LEDs can be obtained.²⁸ We can see that these semipolar LEDs decay faster, which means they have smaller carrier lifetime. Other TRPL measurements also reveal a much smaller carrier lifetime for semipolar LEDs (several hundred picoseconds) compared to that in *c*-plane devices (tens of nanoseconds).²⁹ The current density and carrier density is related as following: $J = qdN/\tau$ where N is the carrier density and τ is the carrier lifetime. Because it takes much less time to decay for carriers, carrier density will be lower at a given current density for semipolar LEDs. Furthermore, recent work in carrier transport indicates that slow tunneling-assisted carrier transport in *c*-plane LEDs results in a large nonuniformity of carrier distribution.³⁰ For semipolar planes, however, a rectangular or close to rectangular barrier shape can be formed, which enables ballistic transport for carriers.³⁰ As a result, carriers are more uniformly distributed in the active region, which may further decrease carrier density in semipolar LEDs and lead to a weaker PSF effect.

Thirdly, due to unbalanced biaxial strain and modified valance band structure, the effective mass of holes will be lower and bandgap will be larger for semipolar QWs compare to that of *c*-plane devices.³¹ This may also play a role in determine the carrier density and PSF effect. Density of states and the carrier density for QWs are given by the follow equations:

$$g(E) = \frac{4\pi m^*}{h^2 d} \quad (3)$$

$$f(E) = \frac{1}{1 + e^{(E-E_f)/kT}} \quad (4)$$

$$\begin{aligned} pn &= \int_{-\infty}^{E_V} g(E)f(E)dE \int_{E_C}^{\infty} g(E)f(E)dE \approx \left[\frac{4\pi m_h^* kT}{h^2 d} e^{\frac{E_V-E_f}{kT}} \right] \left[\frac{4\pi m_e^* kT}{h^2 d} e^{\frac{E_f-E_C}{kT}} \right] \\ &= \frac{16\pi^2 k^2 T^2 (m_h^* m_e^*)}{h^4 d^2} e^{-\frac{E_g}{kT}} \end{aligned} \quad (5)$$

Where m^* is the effective mass m_h^* is the effective mass of holes, m_e^* is the effective mass of electrons, $g(E)$ is the density of states, p is the hole's density, $f(E)$ is the Fermi function, E_f is the Fermi energy, E_V is the energy of valence band edge, E_C is the energy of conduction band edge, d is the QWs thickness, h is the Planck constant, k is the Boltzmann constant and T is the

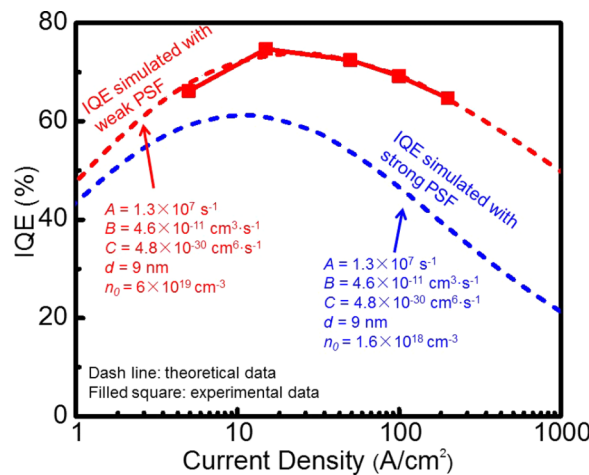


FIG. 6. Experimental efficiency data of semipolar LEDs (filled square). A theoretic fitting for semipolar LEDs with weak PSF effect (dash red line, $n_0 = 6 \times 10^{19} \text{ cm}^{-3}$) and strong PSF effect (solid blue line, $n_0 = 1.6 \times 10^{18} \text{ cm}^{-3}$).

TABLE II. A , B , C , d and n_0 for both c -plane and semipolar InGaN LEDs used in the simulation by modified ABC model.

Planes	$A \times 10^{-7} \text{ (s}^{-1}\text{)}$	$B \times 10^{11} \text{ (cm}^3 \text{ s}^{-1}\text{)}$	$C \times 10^{30} \text{ (cm}^6 \text{ s}^{-1}\text{)}$	$d \text{ (nm)}$	$n_0 \times 10^{-19} \text{ (cm}^{-3}\text{)}$
c^1	0.16	2.8	4.8	15	0.10
c^2	0.08	3.3	2.4	12	0.60
$(30\bar{3}\bar{1})^3$	1.2	4.5	6.0	15	3.0
$(20\bar{2}\bar{1})^4$	0.6	5.0	4.5	12	5.0

¹Reference 33.²Reference 34.³Reference 15.⁴Reference 13.

temperature of the system. The equation shows that the carrier density product pn is proportional to the both electron and hole effective mass, and $\exp(-E_g/kT)$. Park et al found that when incorporating the spontaneous and piezoelectric polarization, semipolar planes have slightly larger bandgap and smaller hole effective mass³⁰ while electron effective mass is almost the same. Therefore, the average carrier density in semipolar InGaN QWs will be lower according to Eq. (5), leading to a weaker PSF effect than c -plane devices. It's worth mentioning that though the carrier density of semipolar LEDs are smaller than c -plane LEDs, the radiative recombination rate, which is Bpn , of the former are much larger due to much better electron and hole wavefunction overlap. In addition, other factors such as weak localization, shorter spontaneous emission lifetime, and larger binding energy of exciton in semipolar LEDs can also lead to a weak PSF effect.³²

III. EXPERIMENTAL RESULTS

Finally, the rate equation model with strong and weak PSF effect is applied to fit the experimental results on a semipolar LEDs¹⁴ as shown in Fig. 6. We assume that the injection efficiency is 100% and light extraction efficiency is 70% which is reasonable with current techniques. It should be noted that A , B , C , d and n_0 coefficient cannot be arbitrarily chosen to fit the data. In real device simulation, it is very important to keep A , B , C coefficients within the reasonable ranges that are reported by theoretical or experimental work, and d is determined by the device structure. As a result we can't choose arbitrary fitting parameters for the work and there's only one set of parameters optimal for specific IQE curve. Due to these constrains, the semipolar LEDs can be only simulated using modified ABC model due to the distinct droop behavior. The IQE curve of semipolar LEDs is well fitted by rate equation model with weak PSF effect where $A = 1.3 \times 10^7 \text{ s}^{-1}$, $B = 4.6 \times 10^{-11} \text{ cm}^3 \cdot \text{s}^{-1}$ and $C = 4.8 \times 10^{-30} \text{ cm}^6 \cdot \text{s}^{-1}$, $d = 9 \text{ nm}$ and $n_0 = 6 \times 10^{19} \text{ cm}^{-3}$ were used. The radiative recombination coefficient is in the reasonable range and is also higher than that of reported c -plane LEDs.^{4,22} This C value is higher than the calculated one possibly due to the accumulative effect of direct (*intraband* and *interband*) and indirect (phonon, alloy or defect assisted transition) Auger recombination process.⁸⁻¹⁰ However, a very large efficiency droop is seen in the IQE curve with strong PSF effect ($n_0 = 1.6 \times 10^{18} \text{ cm}^{-3}$) where the A , B , C and d are the same. These results indicate that by tuning PSF effect we can fit IQE curve of semipolar LEDs extracting A , B , C coefficients which cannot be achieved by conventional ABC model. Table II lists the fitting parameters of modified ABC model for other c -plane and semipolar LEDs.^{13,15,33,34} By comparison, we can see that n_0 of semipolar LEDs are larger than that of c -plane LEDs. Large n_0 must be used in the fitting of semipolar LEDs, which indicates that weak PSF effect may exists in semipolar LEDs which will lead to the low-droop performance. The reasons for this are explained in detail in Sec. III.

IV. CONCLUSIONS

We study the phase-space filling (PSF) effect on the modeling of InGaN LEDs. Very distinct efficiency characteristics were obtained for LEDs with strong (polar) and weak (nonpolar/semipolar)

PSF effect and the physical mechanisms were briefly discussed. By tuning PSF effect, very good agreement between theoretical simulation and experimental result was obtained for the IQE curve for low-droop semipolar LEDs. This result provides a new way to extract important recombination coefficients for semipolar LEDs and may indicate that the low-droop performance is related to the weak PSF effect.

ACKNOWLEDGMENTS

This work is supported by Bisgrove Scholar program from Science Foundation Arizona.

- ¹ M. H. Kim, M. F. Schubert, Q. Dai, J. K. Kim, E. F. Schubert, J. Piprek, and Y. Park, *Appl. Phys. Lett.* **91**, 183507 (2007).
- ² C. C. Pan, Q. Yan, H. Fu, Y. Zhao, Y. R. Wu, C. G. Van de Walle, S. Nakamura, and S. P. DenBaars, *Electron. Lett.* **51**, 1187 (2015).
- ³ E. Kioupakis, P. Rinke, K. T. Delaney, and C. G. Van de Walle, *Appl. Phys. Lett.* **98**, 161107 (2011).
- ⁴ Y. C. Shen, G. O. Müller, S. Watanabe, N. F. Gardner, A. Munkholm, and M. R. Krames, *Appl. Phys. Lett.* **91**, 141101 (2007).
- ⁵ V. Fiorentini, F. Bernardini, F. Della Sala, A. Di Carlo, and P. Lugli, *Phys. Rev. B* **60**, 8849 (1999).
- ⁶ X. Huang, H. Fu, H. Chen, Z. Lu, D. Ding, and Y. Zhao, *J. Appl. Phys.* accepted (2016).
- ⁷ J. Iveland, L. Martinelli, J. Peretti, J. S. Speck, and C. Weisbuch, *Phys. Rev. Lett.* **110**, 177406 (2013).
- ⁸ F. Bertazzi, M. Goano, and E. Bellotti, *Appl. Phys. Lett.* **97**, 231118 (2010).
- ⁹ J. Hader, J. V. Moloney, B. Pasenow, S. W. Koch, M. Sabathil, N. Linder, and S. Lutgen, *Appl. Phys. Lett.* **92**, 261103 (2008).
- ¹⁰ E. Kioupakis, P. Rinke, K. T. Delaney, and C. G. Van de Walle, *Appl. Phys. Lett.* **98**, 161107 (2011).
- ¹¹ H. Y. Ryu, D. S. Shin, and J. I. Shim, *Appl. Phys. Lett.* **100**, 131109 (2012).
- ¹² G. B. Lin, D. Meyaard, J. Cho, E. F. Schubert, H. Shim, and C. Sone, *Appl. Phys. Lett.* **100**, 161106 (2012).
- ¹³ C. C. Pan, S. Tanaka, F. Wu, Y. Zhao, J. S. Speck, S. Nakamura, S. P. DenBaars, and D. Feezell, *Appl. Phys. Express* **5**, 062103 (2012).
- ¹⁴ Y. Zhao, S. Tanaka, C. C. Pan, K. Fujito, D. Feezell, J. S. Speck, S. P. DenBaars, and S. Nakamura, *Appl. Phys. Express* **4**, 082104 (2011).
- ¹⁵ D. L. Becerra, Y. Zhao, S. H. Oh, C. D. Pynn, K. Fujito, S. P. DenBaars, and S. Nakamura, *Appl. Phys. Lett.* **105**, 171106 (2014).
- ¹⁶ H. Fu, Z. Lu, X. Huang, H. Chen, and Y. Zhao, *J. Appl. Phys.* **119**, 174502 (2016).
- ¹⁷ P. Walterweit, O. Brandt, A. Trampert, H. T. Grahn, J. Menniger, M. Ramsteiner, M. Reiche, and K. H. Ploog, *Nature (London)* **406**, 865 (2000).
- ¹⁸ Y. Zhao, J. Sonoda, I. Koslow, C. C. Pan, H. Ohta, J. S. Ha, S. P. DenBaars, and S. Nakamura, *Jpn. J. Appl. Phys.* **49**, 070206 (2010).
- ¹⁹ H. Chen, H. Fu, Z. Lu, X. Huang, and Y. Zhao, *Opt. Express* **24**, A856 (2016).
- ²⁰ A. David and M. J. Grundmann, *Appl. Phys. Lett.* **96**, 103504 (2010).
- ²¹ S. Nakamura and M. R. Krames, *Proc. IEEE* **101**, 2211 (2013).
- ²² E. Kioupakis, Q. Yan, D. Steiauf, and C. G. Van de Walle, *New J. Phys.* **15**, 125006 (2013).
- ²³ J. Hader, J. V. Moloney, and S. W. Koch, *Proc. SPIE* **6115**, 61151T (2006).
- ²⁴ E. Kioupakis, Q. Yan, and C. G. Van de Walle, *Appl. Phys. Lett.* **101**, 231107 (2012).
- ²⁵ Y. Zhao, S. H. Oh, F. Wu, Y. Kawaguchi, S. Tanaka, K. Fujito, J. S. Speck, S. P. DenBaars, and S. Nakamura, *Appl. Phys. Express* **6**, 062102 (2013).
- ²⁶ D. F. Feezell, J. S. Speck, S. P. DenBaars, and S. Nakamura, *J. Disp. Technol.* **9**, 190 (2013).
- ²⁷ H. Fu, Z. Lu, X. Zhao, Y. H. Zhang, S. P. DenBaars, S. Nakamura, and Y. Zhao, *J. Disp. Technol.*, accepted (2015).
- ²⁸ M. Funato, A. Kaneta, Y. Kawakami, Y. Enya, K. Nishizuka, M. Ueno, and T. Nakamura, *Appl. Phys. Express* **3**, 021002 (2010).
- ²⁹ T. Wunderer, P. Bruckner, J. Hertkorn, F. Scholz, G. J. Beirne, M. Jetter, P. Michler, M. Feneberg, and K. Thonke, *Appl. Phys. Lett.* **90**, 171123 (2007).
- ³⁰ D. S. Sizov, R. Bhat, A. Zakharian, K. Song, D. E. Allen, S. Coleman, and C. E. Zah, *IEEE J. Sel. Top. Quantum Electron.* **17**, 1390 (2011).
- ³¹ S. H. Park, *J. Appl. Phys.* **91**, 9904 (2002).
- ³² M. Funato, A. Kaneta, Y. Kawakami, Y. Enya, K. Nishizuka, M. Ueno, and T. Nakamura, *Appl. Phys. Express* **3**, 021002 (2010).
- ³³ K. J. Vampola, N. N. Fellows, H. Masui, S. E. Brinkley, M. Furukawa, R. B. Chung, H. Sato, J. Sonoda, H. Hirasawa, M. Iza, S. P. DenBaars, and S. Nakamura, *Phys. Stat. Sol. A* **206**, 200 (2009).
- ³⁴ Y. Narukawa, M. Ichikawa, D. Sanga, M. Sano, and T. Mukai, *J. Phys. D, Appl. Phys.* **43**, 354002 (2010).